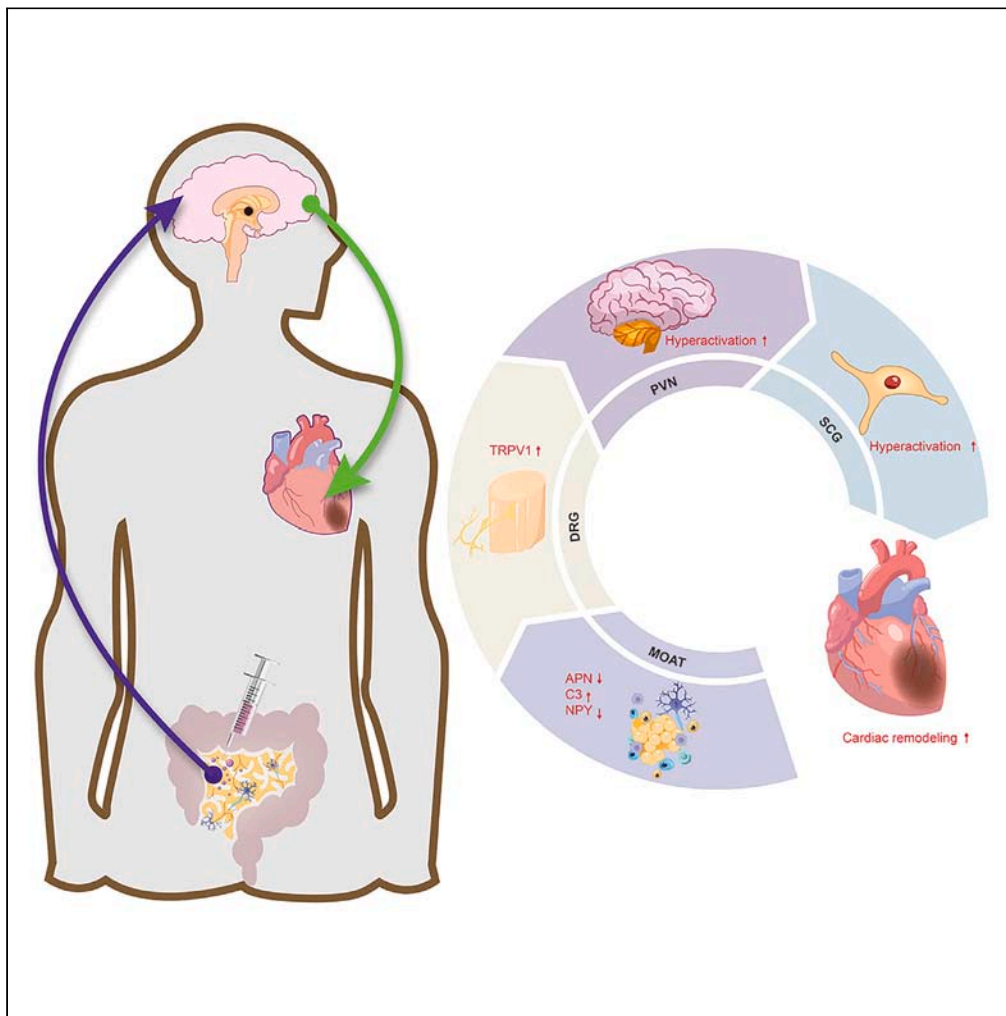**Article**

Blockade of mesenteric and omental adipose tissue sensory neurons improves cardiac remodeling through sympathetic pathway

Jiaxing Huang, Xinyu Liu, Qinfang Qiu, ..., Xiaoya Zhou, Yueyi Wang, Hong Jiang

whuzhouxiaoya@whu.edu.cn (X.Z.)
wangyueyi@whu.edu.cn (Y.W.)
hong-jiang@whu.edu.cn (H.J.)

Highlights

MI leads to alterations in the secretory and inflammatory profiles of MOAT

MOAT contributes to abnormal afferent and brain-heart sympathetic axis

MOAT sensory afferent denervation has cardioprotective effects

MOAT intervention as a cardioprotective strategy may provide clinical benefits

iScience

Article

Blockade of mesenteric and omental adipose tissue sensory neurons improves cardiac remodeling through sympathetic pathway

Jiaxing Huang,[1,2] Xinyu Liu,[1,2] Qinfang Qiu,[1] Wuping Tan,[1] Rui Li,[1] Haosong Xi,[1] Chen Peng,[1] Liping Zhou,[1] Xiaoya Zhou,[1,*] Yueyi Wang,[1,*] and Hong Jiang[1,3,*]

SUMMARY

Mesenteric and omental adipose tissue (MOAT) communicates directly with the heart through the secretion of bioactive molecules and indirectly through afferent signaling to the central nervous system. Myocardial infarction (MI) may induce pathological alterations in MOAT, which further affects cardiac function. Our study revealed that MI induced significant MOAT transcriptional changes in genes related with signal transduction, including adiponectin (*APN*), neuropeptide Y (*NPY*), and complement C3 (*C3*), potentially influencing afferent activity. We further found that MOAT sensory nerve denervation with capsaicin (CAP) prevented cardiac remodeling, improved cardiac function, and reversed cardiac sympathetic nerve hyperactivation in the MI group, accompanied by reduced serum norepinephrine. In addition, CAP reversed the elevated MOAT afferent input and brain-heart sympathetic outflow post-MI, increasing APN and NPY and decreasing C3 and serum proinflammatory factors. These results demonstrated that blockade of the MOAT afferent sensory nerve exerts a cardioprotective effect by inhibiting the brain-heart sympathetic axis.

INTRODUCTION

Myocardial infarction (MI) is the leading cause of death worldwide. With advancements in treatment options, the survival rate has increased significantly; however, there is still room for improvement in preventing adverse cardiac remodeling. MI is accompanied by sympathetic nervous system (SNS) activation,[1] which has clinical implications by altering adipokines and inflammatory markers via sympathetic innervation.[2,3] Excessive activation of SNS post-MI further promotes cardiac function deterioration and disease progression. Our previous studies have confirmed the existence of the cardiac sympathetic excitation axis,[4,5] which extends from the hypothalamic paraventricular nucleus (PVN), a central regulatory hub for sympathetic outflow, to the superior cervical ganglion (SCG), a sympathetic ganglion innervating the heart.[6] Inhibition of the PVN-SCG-heart sympathetic axis is crucial for preventing adverse cardiac outcomes following MI.

Clinical data suggest a complex relationship between human adipose tissue and cardiovascular disease,[7] including the obesity paradox. Accumulation of body mass is a risk factor for MI, but it is associated with a better prognosis compared to non-overweight/obese patients, partly due to the altered secretomic profile and inflammatory status of adipose tissue under pathological conditions.[8] However, the relationship between adipose tissue and cardiac disease in non-overweight patients and the potential feedback has rarely been studied. Clinical studies have shown that patients with MI exhibit an adipokine imbalance, with significantly lower adiponectin (APN) and higher leptin levels, especially in patients with visceral obesity.[9] APN is a classic anti-inflammatory agent that regulates thermal nociceptive sensitivity via the transient receptor potential cation channel subfamily V member 1 (TRPV1) of sensory neurons in the dorsal root ganglion (DRG).[10] The decreased APN corresponds to an increased incidence of neuropathic pain in post-MI patients,[11] which further complicates disease progression.

Visceral adiposity has a detrimental effect on the cardiometabolic risk profile.[12] Neuroanatomical and functional evidence suggests that visceral adipose tissue (VAT) is innervated by the sympathetic nerve, which also possesses sensory afferent nerve endings.[13–15] Activation of the SNS through VAT afferent activity is associated with obesity and hypertension.[16,17] Pharmacological ablation with capsaicin (CAP) or anatomical denervation can provide hypertensive benefits via VAT-PVN sympathetic inhibition but not under normal conditions.[18,19] However, the anatomical location of adipose depots determines their specific function. Previous studies have primarily focused on inguinal, perirenal, and retroperitoneal adipose tissue as well as the central projection in the PVN through the DRG.[20] Few studies have examined mesenteric or omental adipose tissue. Furthermore, the effect of VAT afferent feedback on the heart post-MI remains unclear, despite the potential cardioprotective effects of VAT afferent inhibition through modification of abnormal PVN cardiac sympathetic efferent outflow. Research on the

sympathetic interaction between mesenteric and omental adipose tissue (MOAT) and the heart can elucidate the underlying mechanism and promote the further development of a valuable therapeutic strategy for pathological conditions.

VAT communicates directly with the heart through bioactive molecule secretion, and indirectly through afferent signaling to the central nervous system. The above evidence suggests that VAT afferent nerves may influence the "PVN-SCG-heart" sympathetic axis. This study aimed to investigate transcriptional alterations in MOAT following MI and explore their potential influence on cardiac function. Additionally, this study sought to determine whether MOAT afferent intervention can be cardioprotective through modification of the abnormal PVN sympathetic efferent outflow to the heart. These results could provide insights into the pathological status of MI and lead to the development of cardioprotective strategies with potential clinical therapeutic benefits.

RESULTS

Alterations in the transcriptional status of MOAT after MI

We assessed the transcriptional changes in MOAT two weeks after MI using RNA-seq in MOAT samples from the MI and Sham groups. Differentially expressed genes (DEGs) were identified to further investigate the effect of MI on MOAT. Principal component analysis (PCA) of the RNA-seq data revealed significant differences in gene signatures between the two groups (Figure S1A). The volcano plot and heatmap of the data showed 240 upregulated genes and 513 downregulated genes in the MI group compared to the Sham group (Figures 1A and 1B). Kyoto Encyclopedia of Genes and Genomes (KEGG) pathway analysis revealed that MI onset significantly altered genes related to "environmental information processing", particularly in the "signal transduction" and "signaling molecules and interactions" categories (Figure 1C). Additionally, significant alterations were observed in the "Endocrine system" genes within the "Organismal Systems" category. Figures S1B–S1D present the results of Gene Ontology (GO) enrichment analysis and a table of significantly upregulated and downregulated genes. We then used the KEGG enrichment method to analyze the altered genes and found that the peroxisome proliferator-activated receptor (PPAR) signaling pathway was the most significantly enriched pathway (Figure 1D). The PPAR signaling pathway, identified through the KEGG enrichment method, comprised 12 genes, including *APN*, *Lpl*, *Plin1*, *Plin4*, *Acsl1*, and *Fabp4*, most of which were lipolysis-related genes, and *APN* was the only adipokine. *APN* was one of the most significantly altered genes in the PPAR signaling pathway. Gene Set Enrichment Analysis (GSEA) of the PPAR signaling pathway revealed that *APN* was a core gene involved in mediating alteration in MOAT post MI (Figure S1E). Additionally, *APN* also belonged to the "Endocrine system" category in the KEGG pathway analysis. Subsequently, we studied the neuroactive ligand-receptor interaction with the largest number of altered genes in the KEGG enrichment analysis, including 17 genes such as *C3*, *NPY*, *Adrb3*, *Mc2r*, *Tshr*, *Ptger3*, *P2rx2*, and *Agt*. Among these genes, neuropeptide Y (*NPY*) and complement C3 (*C3)* have been shown to activate sensory afferent nerves through direct activation or neuroinflammation. Given that *APN*, *NPY*, and *C3* have been documented to increase sensory neuron afferent inputs, we further investigated the effect of MOAT sensory nerve denervation (MOAT-D) on the heart after MI.

MOAT-D alleviated cardiac remodeling after MI

CAP microinjection was used to block the sensory afferent nerves of MOAT. The experimental protocol is illustrated in Figure 2A. Normal-weight rats were used to eliminate the potential confounding effects of obesity, and there was no significant difference in body weight before and after the intervention (Figure S1F). Masson's staining was used to detect myocardial fibrosis (Figure 2B). The findings revealed that MI induced cardiac fibrosis, which was significantly reversed by CAP (Figure 2C). The MI group exhibited a higher number of TUNEL-positive cells than the Sham group and CAP treatment significantly decreased apoptosis (Figures S3A and S3B). Subsequently, the effect of MOAT-D on post-MI cardiac function was evaluated by echocardiography in MI rats at 2 and 4 weeks, as shown in Figure 2C. Left ventricular systolic function was significantly impaired after MI, as evidenced by significant decreases in ejection fraction (EF) and fractional shortening (FS). The CAP group showed significant improvements compared with the MI group, indicating the beneficial effect of MOAT-D on post-MI cardiac function (Figures 2D and 2E). Additionally, MI significantly increased left ventricular internal dimension (LVID), including systolic LVID (LVIDs) and diastolic LVID (LVIDd) compared to the Sham group, which were attenuated in CAP group (Figures 2F and 2G). In addition, we observed the same cardioprotective effect at four weeks postoperatively (Figures S2A–S2E). These findings suggested that CAP significantly improved MI-induced cardiac dysfunction.

MOAT-D attenuated systemic sympathetic activity after MI

We assessed the effect of MOAT-D on the autonomic nervous system by measuring heart rate variability (HRV) to reflect cardiac autonomic function and used ELISA to evaluate serum norepinephrine (NE) levels as a marker of systemic sympathetic activity. The MI group exhibited increased low frequency (LF) power, LF/high frequency (HF) power ratio, and decreased HF power compared to the Sham group, indicating heightened sympathetic modulation and diminished parasympathetic tone following MI. However, these changes were mitigated in the CAP group (Figures 3A–3C). Furthermore, as depicted in Figure 3D, the serum levels of NE in the MI group were significantly elevated compared with those in the Sham group, whereas the CAP group showed alleviation of this alteration. Similarly, the CAP group also displayed an improvement in systemic sympathetic hyperactivity four weeks after the operation (Figures S2F–S2H).

MOAT-D inhibited SCG activation and remodeling after MI

Since the SCG serves as a crucial cardiac sympathetic ganglion, we further evaluated its function and remodeling.[21] Our findings revealed a reduction in the proportion of c-fos-positive neurons in the SCG of the CAP group, suggesting that MOAT-D inhibited SCG activation and
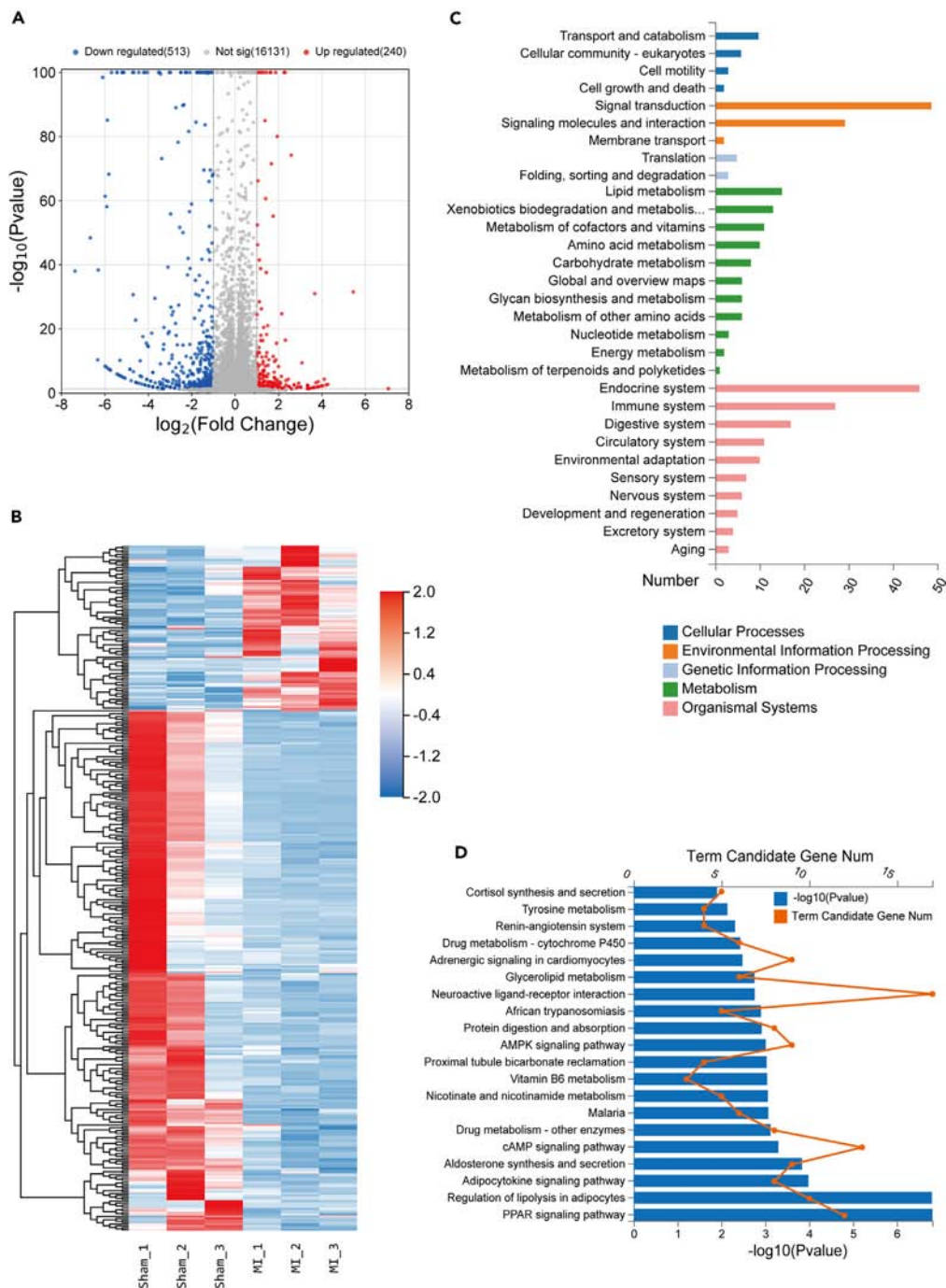
Figure 1. Transcriptional alterations in MOAT after MI

(A, B) Volcano plot (A) and heatmap (B) showing upregulated or downregulated DEGs in MOAT induced by MI.

(C) KEGG pathway classification of DEGs altered by MI.

(D) KEGG enrichment between Sham and MI groups. Q-values <0.05. MI, myocardial infarction; DEGs, differentially expressed genes; KEGG, Kyoto Encyclopedia of Genes and Genome; Q-value, FDR-adjusted p-value.

outflow to the heart (Figures 4A and 4B). Studies have demonstrated morphological and neurochemical remodeling in the cardiac sympathetic ganglion after MI.[22–25] Immunohistochemical staining was performed to evaluate the intensity of tyrosine hydroxylase (TH) and choline acetyltransferase (ChAT) neurons in the SCG four weeks after MI to assess neurochemical remodeling. TH positivity represented adrenergic neurons, whereas ChAT positivity represented cholinergic neurons. Representative images from each group are shown in Figure 4C. Our
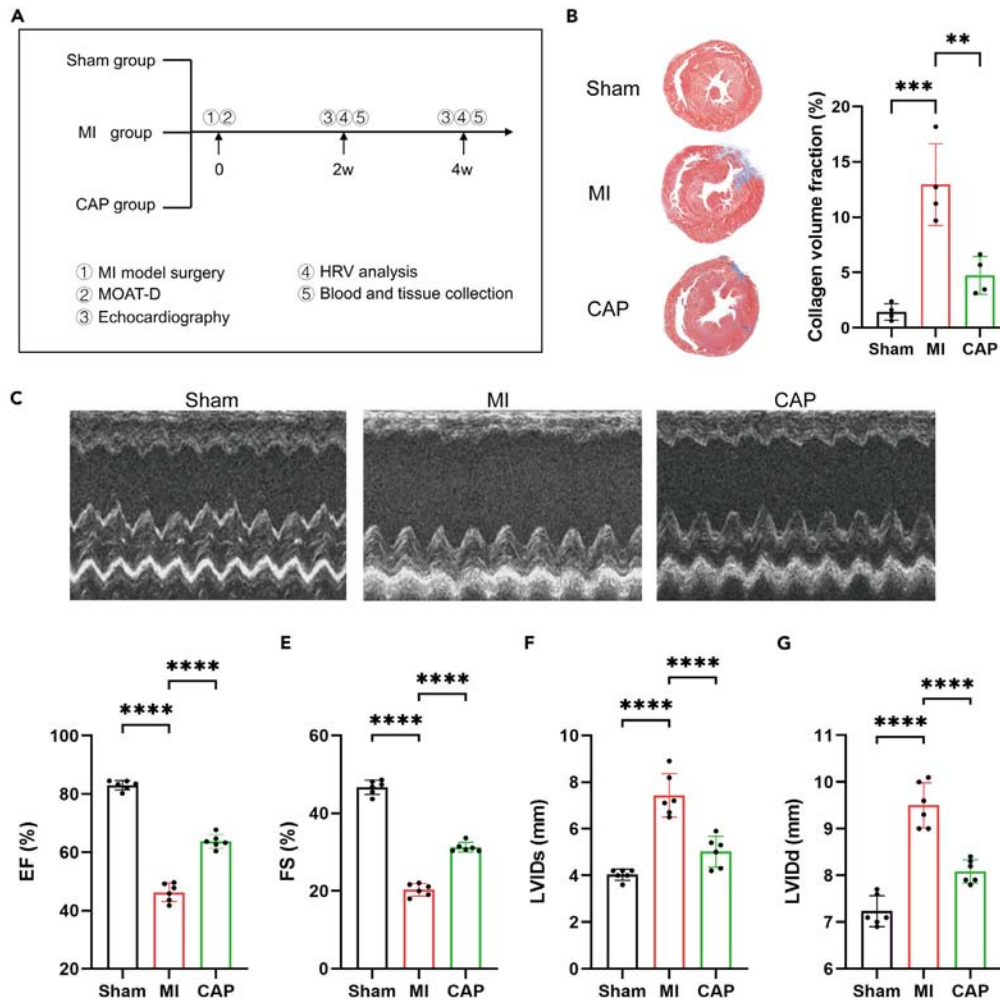
Figure 2. MOAT-D improved cardiac dysfunction and cardiac remodeling after MI

(A) Experimental protocol. Modeling and intervention were performed simultaneously, with samples taken at 2 and 4 weeks to observe cardiac remodeling, cardiac sympathetic nervous system, and ganglion remodeling, respectively.

(B) Representative images and quantitative analysis of Masson's staining in all groups.

(C–G) Representative images and echocardiography analysis for EF (D), FS (E), LVIDs (F), and LVIDd (G) in the three groups. MI, myocardial infarction; CAP, capsaicin; MOAT-D, mesenteric and omental adipose tissue sensory nerve denervation; HRV, heart rate variability; EF, ejection fraction; FS, fractional shortening; LVIDs, left ventricular internal dimension (systole); LVIDd, left ventricular internal dimension (diastole); $**p < 0.01$, $***p < 0.001$, $****p < 0.0001$. One-way ANOVA analysis with Tukey's multiple comparisons test was used for normally distributed statistical analysis. Values represent mean $\pm$ SD.

results indicated that the intensity of TH and ChAT neurons in the MI group was significantly higher than that in the Sham group (Figures 4D and 4E). However, the CAP group showed a marked reversal of this change, suggesting an inhibitory effect of MOAT-D on neurochemical remodeling in the SCG post MI.

MOAT-D exhibited inhibited DRG activation and modulated the brain-heart sympathetic axis after MI

We further investigated the MOAT sensory afferent transmission. qRT-PCR revealed a significant increase in the expression of the transmitter calcitonin gene-related peptide (CGRP) in the DRG after MI, indicating sensory afferent pathway activation. In contrast, the CGRP levels were suppressed in the CAP group (Figure 5A). Western blot analysis revealed a trend consistent with the qRT-PCR results (Figures 5B and 5C). Immunohistochemical analysis showed that TRPV1 expression increased significantly in the DRG after MI and was restored by CAP treatment (Figures 5D and 5E). Furthermore, immunofluorescence labeling was used to determine the proportion of c-fos-positive neurons in the PVN. As depicted in Figure 5F, a significant increase in c-fos-positive neurons in the PVN was observed in the MI group compared to the Sham group, indicating enhanced central sympathetic activation and outflow following MI. However, this upregulation was ameliorated in the CAP group (Figure 5G). These findings suggested that MOAT-D significantly inhibited DRG and PVN activation.
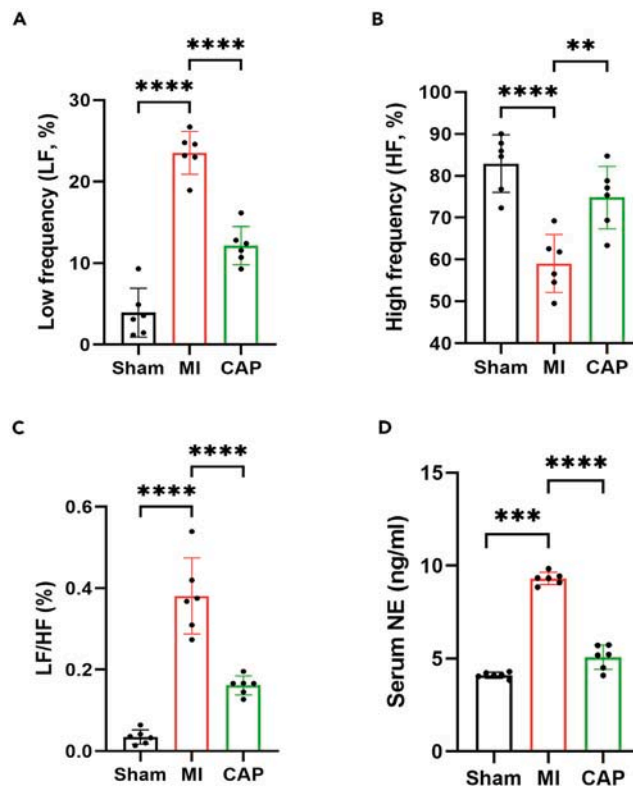
Figure 3. MOAT-D inhibited systemic sympathetic activity after MI

(A–C) Spectral analysis of HRV reflecting cardiac sympathetic activity: LF (A), HF (B), and the ratio of LF/HF (C).

(D) Differences in serum NE levels. MI, myocardial infarction; HRV, heart rate variability; CAP, capsaicin; LF, low frequency (0.20–0.75 Hz); HF, high frequency (0.75–0.2 Hz); LF/HF, ratio of LF to HF; NE, norepinephrine; $**p < 0.01$, $***p < 0.001$, $****p < 0.0001$. One-way ANOVA analysis with Tukey's multiple comparisons test was used for normally distributed statistical analysis. Values represent mean $\pm$ SD.

MOAT-D modulated PPAR signaling pathway and systemic inflammation after MI

Compared with the Sham group, the mRNA and protein expression levels of APN in the MOAT decreased significantly after MI, which was reversed by CAP treatment (Figures 6A and 6B). We further examined the mRNA and protein expression levels of C3 and NPY. The results showed that the mRNA and protein expression levels of C3 in MOAT were significantly increased after MI, while NPY were significantly decreased. However, the mRNA expression of C3 and the protein expression of C3 and NPY was restored by CAP (Figures 6C–6F). Subsequently, we assessed systemic inflammation by measuring serum levels of IL-6 and TNF-α using ELISA. As shown in Figures 6H and 6I, the inflammatory markers in the serum of the MI group were significantly elevated, whereas the CAP group exhibited markedly lower inflammation than the MI group.

DISCUSSION

The present study revealed that MOAT exhibited significant alterations in genes associated with neuronal signal transduction and the endocrine system following MI, which might trigger a positive feedback loop and enhance the cardiac sympathetic outflow. Indeed, MOAT sensory afferent denervation presented a significant potential to attenuate excessive cardiac sympathetic overactivation post-MI, thereby restoring cardiac function and alleviating cardiac remodeling. These findings reveal crosstalk between MOAT and the heart, emphasizing the cardioprotective effect of MOAT sensory afferent intervention through the brain-heart sympathetic axis.

MOAT represents a crucial component of human VAT,[26] but its biological functions during the pathological state of MI are not fully understood. A recent study reported that myocardial ischemia/reperfusion-induced plasma extracellular vesicles release can cause endoplasmic reticulum stress and endocrine dysfunction in adipocytes.[27] Furthermore, activated immune cells (dendritic cells) post-MI can migrate to the epicardial adipose tissue and release cytokines and growth factors.[28] In addition, MI-related SNS overactivation signals to the integration center of the PVN, thereby triggering MOAT sympathetic outflow. These circulatory, metabolic, and sympathetic abnormalities post-MI might directly affect MOAT. To evaluate these effects, bulk RNA sequencing was used to identify significant alterations in the MOAT transcriptome induced by MI. KEGG enrichment analysis of the modified genes revealed that MI significantly altered the PPAR signaling pathway, neuroactive ligand-receptor interaction, lipolysis regulation in adipocytes, and adipocytokine signaling pathway in MOAT. Using GSEA of the
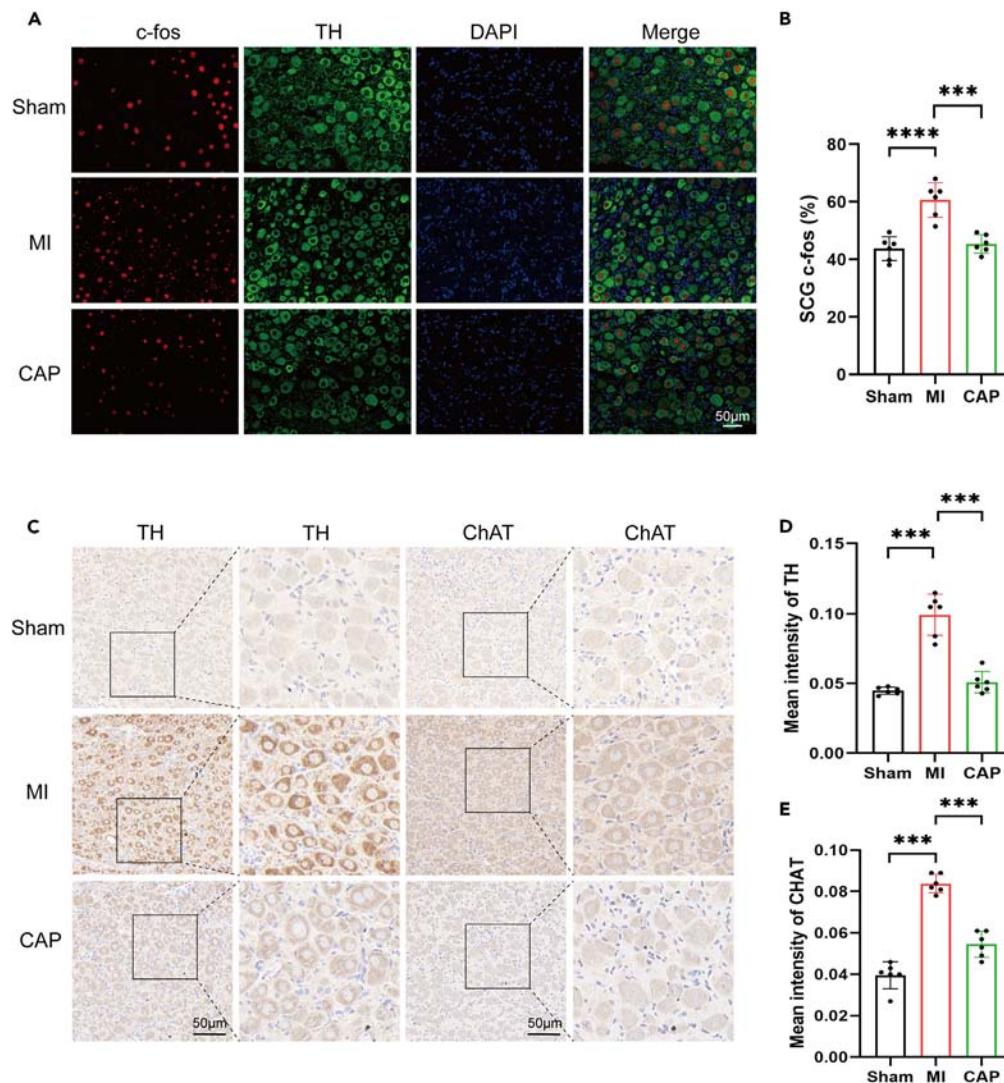
Figure 4. MOAT-D suppressed SCG hyperactivation and remodeling after MI

(A) Representative immunofluorescence staining of c-fos in the SCG of all groups. Scale bar = 50 μm.

(B) The percentage of c-fos-positive neurons in TH$^+$-stained neurons.

(C) Representative images of TH and ChAT expression assessed by immunohistochemistry in the SCG. Scale bar = 50 μm.

(D and E) Quantitative data on the expression of TH and ChAT in SCG. MI, myocardial infarction; CAP, capsaicin; TH, tyrosine hydroxylase; ChAT, choline acetyltransferase; SCG, superior cervical ganglion; DAPI, 4′,6-diamidino-2-phenylindole; ***p < 0.001, ****p < 0.0001. One-way ANOVA analysis with Tukey's multiple comparisons test was used for normally distributed statistical analysis. Values represent mean ± SD.

PPAR signaling pathway, we identified *APN* as a central gene. Additionally, we screened significantly altered genes related to neural signal transduction in the context of neuroactive ligand-receptor interactions, including *APN*, *NPY*, and *C3*, which have also been reported to influence sensory afferent activity.[29–32] Consistently, we observed significantly reduced relative mRNA expression of APN and NPY and increased C3 in MOAT following MI, which corresponded to protein expression. These findings suggest an abnormal neural afferent activity in the MOAT.

Recent studies have established a close connection between white adipose tissue (WAT) and SNS.[16] Activation of afferent neurons in the same-sided adipose tissue increases sympathetic nerve outflow to the bilateral testicular adipose tissue.[33] Additionally, increased sensory neuron activity in inguinal WAT has been found to result in higher renal sympathetic nerve activity.[34] Neuroanatomical and neurophysiological studies have provided evidence that the VAT afferent nerve signal is transmitted by the DRG to the PVN, which serves as the central hub for sympathetic nerve outflow.[13,14] For instance, the injection of lidocaine into the PVN can block the elevation of renal sympathetic nerve activity and blood pressure caused by adipose tissue afferent nerve activation.[18] In addition, our previous research showed that PVN-SCG facilitates
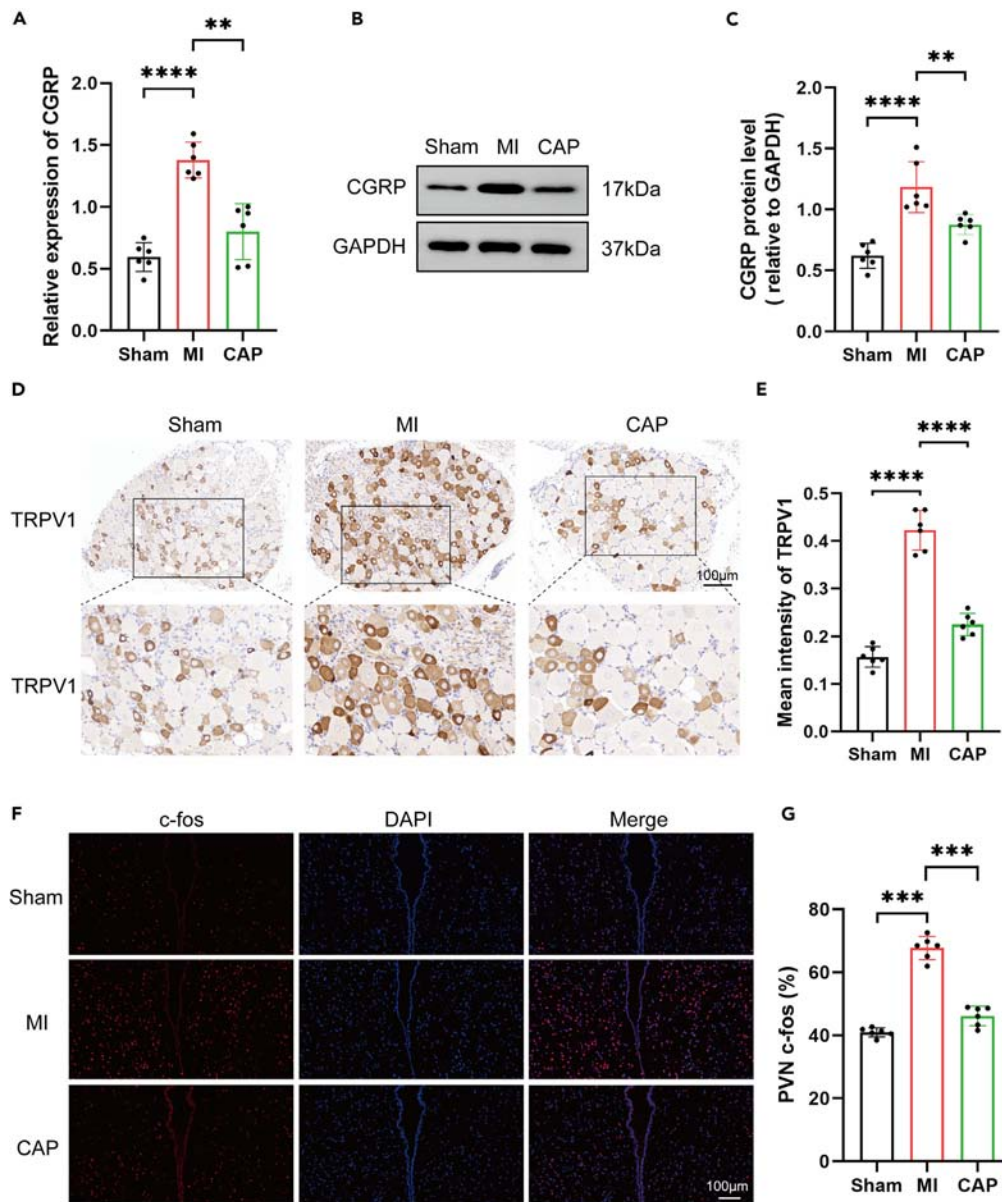
Figure 5. MOAT-D inhibited DRG hyperactivation and modulated the brain-heart sympathetic axis after MI

(A) Relative CGRP mRNA expression.

(B) Representative images of western blotting of CGRP expression in all groups.

(C) Relative protein expression of CGRP normalized to GAPDH.

(D) Representative images of TRPV1 expression assessed by immunohistochemistry in the DRG. Scale bar = 100 μm.

(E) Quantitative data on the expression of TRPV1 in DRG.

(F) Representative immunofluorescence staining of c-fos in the PVN of all the groups. Scale bar = 100 μm.

(G) Quantitative analysis of c-fos-expressing neurons as the percentage of DAPI-stained neurons. MI, myocardial infarction; CAP, capsaicin; TRPV1, transient receptor potential cation channel subfamily V member 1; PVN, paraventricular nucleus; DAPI, 4′,6-diamidino-2-phenylindole; CGRP, calcitonin gene-related peptide; GAPDH, glyceraldehyde-3-phosphate dehydrogenase; $**p < 0.01$, $***p < 0.001$, $****p < 0.0001$. One-way ANOVA analysis with Tukey's multiple comparisons test was used for normally distributed statistical analysis. Values represent mean ± SD.

cardiac sympathetic overactivity post-MI.[5] In this study, we hypothesized that, following MI, MOAT afferent signal activation triggers cardiac SNS activation via the DRG-PVN-SCG neural circuit. Indeed, treatment with CAP (MOAT denervation) significantly reduced CGRP expression in the DRG and neural overactivation in the PVN and SCG post-MI, indicating suppression of MOAT afferent input and cardiac sympathetic outflow, thereby exerting a cardioprotective effect.
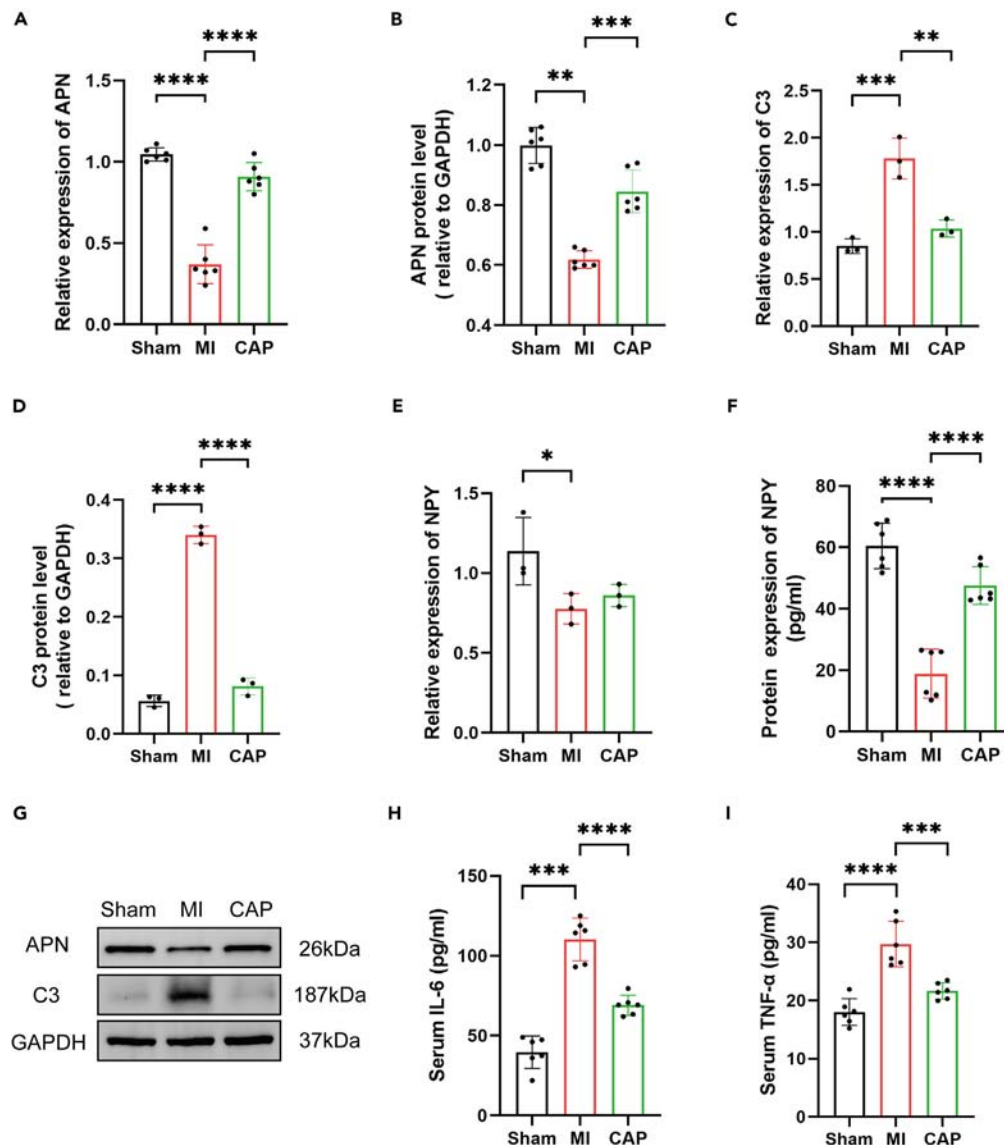
Figure 6. MOAT-D modulated PPAR signaling pathway and systemic inflammation after MI

(A) Relative APN mRNA expression levels.

(B) Western blot analysis of APN expression in all groups.

(C) Relative C3 mRNA expression levels.

(D) Western blot analysis of C3 expression in all groups.

(E) Relative NPY mRNA expression levels.

(F) ELISA analysis of APN protein expression in all groups.

(G) Representative images of western blot analysis in all groups.

(H and I) Pro-inflammatory TNF-α and IL-6 levels in plasma are shown for different groups. MI, myocardial infarction; CAP, capsaicin; APN, adiponectin; C3, complement C3; NPY, neuropeptide Y; IL-6, interleukin-6; TNF-α, tumor necrosis factor-α; GAPDH, glyceraldehyde-3-phosphate dehydrogenase; *$p < 0.05$, **$p < 0.01$, ***$p < 0.001$, ****$p < 0.0001$. One-way ANOVA analysis with Tukey's multiple comparisons test was used for normally distributed statistical analysis. Values represent mean $\pm$ SD.

The cardiac sympathetic nerves are primarily regulated by the PVN-SCG-heart sympathetic axis.[4] The PVN serves as the central hub for sympathetic nerve outflow, while the SCG supplies postganglionic cardiac sympathetic nerves. Modulation of this axis suppresses excessive activation of the cardiac sympathetic nerves.[35] C-Fos functions as a marker of neuronal activation. Previous studies have reported significantly increased c-fos activity in both the PVN and SCG post MI,[4,5,35] which is consistent with the findings of this study. Elevated c-fos activity leads to excessive activation of the cardiac SNS and adverse cardiac outcomes.[36,37] In this study, CAP administration significantly reduced c-fos activity in both the PVN and SCG, indicating restrained cardiac SNS overactivation. Additionally, the SCG experienced neurochemical changes after

MI. In a canine MI model, the cardiac sympathetic ganglion showed increased TH neuron intensity, but there was no significant difference in ChAT neurons.[25,38] In non-ischemic heart failure rat models, SCG neurons undergo a phenotypic shift from adrenergic to cholinergic.[39] Our findings indicate that blocking sensory input from the MOAT improves SCG neuron remodeling. CAP treatment reversed the increased TH intensity in SCG neurons post-MI and downregulated the phenotypic transition of SCG neurons from adrenergic to cholinergic activity.

APN is a crucial adipokine secreted by MOAT. Clinical investigations have revealed a significant reduction in APN levels post-MI, which is consistent with the findings of our study on MOAT.[40] APN regulates thermal nociception afferents in both physiological and neuropathic pain states via modulation of TRPV1 receptor and CGRP release in DRG.[32] In our study, CAP administration in MOAT post-MI reduced CGRP and TRPV1 in the DRG, signifying the suppression of the MOAT sensory afferent signal. Furthermore, our transcriptomic analysis revealed significant upregulation of *C3* and downregulation of *NPY* in MOAT post-MI. Given that C3 has been reported to increase TRPV1 expression and NPY inhibits TRPV1-mediated sensory neuron activation and suppresses CGRP neuronal release,[30,31] these findings revealed increased sensory afferent input. The possible mechanism involved reduced APN and NPY and increased C3 within the MOAT post-MI, resulting in CGRP release and TRPV1 overexpression that activates DRG and sensory afferent signals, which in turn participate in cardiac sympathetic overactivation via the "DRG-PVN-SCG" pathway. Therefore, CAP effectively blocked sensory afferent input, reduced CGRP release, and TRPV1 overexpression in the DRG, and simultaneously downregulated brain-heart sympathetic outflow.

Limitations of the study

The study had several limitations. First, the animals used in this study were male, and females may exhibit different receptor expression, hormone levels, and drug responses. Second, we only focused on the specific genes that were altered in the MI group and did not conduct RNA sequencing of the MOAT in the CAP group. Given the complexity of the sympathetic afferent feedback loop, the MOAT was influenced by the multiple and complex processes involved in the sensory afferent blockade-related sympathetic innervation of both the heart and MOAT itself, and the rescued cardiac severity also contributed to moderate MOAT pathological changes. The details of CAP-induced modifications remain unknown. Therefore, further studies are required to understand these underlying effects.

STAR★METHODS

Detailed methods are provided in the online version of this paper and include the following:

- KEY RESOURCES TABLE
- RESOURCE AVAILABILITY
  - Lead contact
  - Materials availability
  - Data and code availability
- EXPERIMENTAL MODEL AND STUDY PARTICIPANT DETAILS
  - Animals
- METHOD DETAILS
  - Experimental protocols
  - Establishment of MI model
  - MOAT sensory nerve denervation (MOAT-D)
  - Echocardiography
  - Measurement of the HRV
  - Histological assessment
  - qRT-PCR analysis
  - RNA sequencing (RNA-Seq)
  - ELISA
  - Western blotting
- QUANTIFICATION AND STATISTICAL ANALYSIS
  - Statistical analysis

SUPPLEMENTAL INFORMATION

Supplemental information can be found online at https://doi.org/10.1016/j.isci.2024.110245.

REFERENCES

1. Ciarka, A., van de Borne, P., and Pathak, A. (2008). Myocardial infarction, heart failure and sympathetic nervous system activity: new pharmacological approaches that affect neurohumoral activation. Expert Opin. Investig. Drugs 17, 1315–1330. https://doi.org/10.1517/13543784.17.9.1315.

2. Martinez-Sanchez, N., Sweeney, O., Sidarta-Oliveira, D., Caron, A., Stanley, S.A., and Domingos, A.I. (2022). The sympathetic nervous system in the 21st century: Neuroimmune interactions in metabolic homeostasis and obesity. Neuron 110, 3597–3626. https://doi.org/10.1016/j.neuron.2022.10.017.

3. Hao, S., Sui, X., Wang, J., Zhang, J., Pei, Y., Guo, L., and Liang, Z. (2021). Secretory products from epicardial adipose tissue induce adverse myocardial remodeling after myocardial infarction by promoting reactive oxygen species accumulation. Cell Death Dis. 12, 848. https://doi.org/10.1038/s41419-021-04111-x.

4. Jiao, L., Wang, Y., Zhang, S., Wang, Y., Liu, Z., Liu, Z., Zhou, Y., Zhou, H., Xu, X., Li, Z., et al. (2022). Melatonin improves cardiac remodeling and brain-heart sympathetic hyperactivation aggravated by light disruption after myocardial infarction. J. Pineal Res. 73, e12829. https://doi.org/10.1111/jpi.12829.

5. Wang, Y., Jiang, W., Chen, H., Zhou, H., Liu, Z., Liu, Z., Liu, Z., Zhou, Y., Zhou, X., Yu, L., and Jiang, H. (2021). Sympathetic Nervous System Mediates Cardiac Remodeling After Myocardial Infarction in a Circadian Disruption Model. Front. Cardiovasc. Med. 8, 668387. https://doi.org/10.3389/fcvm.2021.668387.

6. Ziegler, K.A., Ahles, A., Wille, T., Kerler, J., Ramanujam, D., and Engelhardt, S. (2018). Local sympathetic denervation attenuates myocardial inflammation and improves cardiac function after myocardial infarction in mice. Cardiovasc. Res. 114, 291–299. https://doi.org/10.1093/cvr/cvx227.

7. Lavie, C.J., Milani, R.V., and Ventura, H.O. (2009). Obesity and cardiovascular disease: risk factor, paradox, and impact of weight loss. J. Am. Coll. Cardiol. 53, 1925–1932. https://doi.org/10.1016/j.jacc.2008.12.068.

8. Antonopoulos, A.S., and Tousoulis, D. (2017). The molecular mechanisms of obesity paradox. Cardiovasc. Res. 113, 1074–1086. https://doi.org/10.1093/cvr/cvx106.

9. Barbarash, O., Gruzdeva, O., Uchasova, E., Dyleva, Y., Belik, E., Akbasheva, O., Karetnikova, V., and Kokov, A. (2016). The role of adipose tissue and adipokines in the manifestation of type 2 diabetes in the long-term period following myocardial infarction. Diabetol. Metab. Syndr. 8, 24. https://doi.org/10.1186/s13098-016-0136-6.

10. From the American Association of Neurological Surgeons AANS American Society of Neuroradiology ASNR Cardiovascular and Interventional Radiology Society of Europe CIRSE Canadian Interventional Radiology Association CIRA Congress of Neurological Surgeons CNS European Society of Minimally Invasive Neurological Therapy ESMINT European Society of Neuroradiology ESNR European Stroke Organization ESO Society for Cardiovascular Angiography and Interventions SCAI Society of Interventional Radiology SIR Society of NeuroInterventional Surgery SNIS and World Stroke Organization WSO, Sacks, D., Baxter, B., Campbell, B.C.V., Carpenter, J.S., Cognard, C., Dippel, D., Eesa, M., Fischer, U., Hausegger, K., et al. (2018). Multisociety Consensus Quality Improvement Revised Consensus Statement for Endovascular Therapy of Acute Ischemic Stroke. Int. J. Stroke 13, 612–632. https://doi.org/10.1177/1747493018778713.

11. Ziegler, D., Rathmann, W., Meisinger, C., Dickhaus, T., and Mielck, A.; KORA Study Group (2009). Prevalence and risk factors of neuropathic pain in survivors of myocardial infarction with pre-diabetes and diabetes. The KORA Myocardial Infarction Registry. Eur. J. Pain 13, 582–587. https://doi.org/10.1016/j.ejpain.2008.07.007.

12. Fox, C.S., Massaro, J.M., Hoffmann, U., Pou, K.M., Maurovich-Horvat, P., Liu, C.Y., Vasan, R.S., Murabito, J.M., Meigs, J.B., Cupples, L.A., et al. (2007). Abdominal visceral and subcutaneous adipose tissue compartments: association with metabolic risk factors in the Framingham Heart Study. Circulation 116, 39–48. https://doi.org/10.1161/circulationaha.106.675355.

13. Bartness, T.J., Kay Song, C., Shi, H., Bowers, R.R., and Foster, M.T. (2005). Brain-adipose tissue cross talk. Proc. Nutr. Soc. 64, 53–64. https://doi.org/10.1079/pns2004409.

14. Bartness, T.J., Shrestha, Y.B., Vaughan, C.H., Schwartz, G.J., and Song, C.K. (2010). Sensory and sympathetic nervous system control of white adipose tissue lipolysis. Mol. Cell. Endocrinol. 318, 34–43. https://doi.org/10.1016/j.mce.2009.08.031.

15. Underwood, E. (2021). A sense of self. Science 372, 1142–1145. https://doi.org/10.1126/science.372.6547.1142.

16. Xiong, X.-Q., Chen, W.-W., and Zhu, G.-Q. (2014). Adipose afferent reflex: sympathetic activation and obesity hypertension. Acta Physiol. 210, 468–478. https://doi.org/10.1111/apha.12182.

17. Esler, M., Straznicky, N., Eikelis, N., Masuo, K., Lambert, G., and Lambert, E. (2006). Mechanisms of sympathetic activation in obesity-related hypertension. Hypertension 48, 787–796. https://doi.org/10.1161/01.Hyp.0000242642.42177.49.

18. Xiong, X.-Q., Chen, W.-W., Han, Y., Zhou, Y.-B., Zhang, F., Gao, X.-Y., and Zhu, G.-Q. (2012). Enhanced Adipose Afferent Reflex Contributes to Sympathetic Activation in Diet-Induced Obesity Hypertension. Hypertension 60, 1280–1286. https://doi.org/10.1161/HYPERTENSIONAHA.112.198002.

19. Garcia, M.L., Milanez, M.I.O., Nishi, E.E., Sato, A.Y.S., Carvalho, P.M., Nogueira, F.N., Campos, R.R., Oyama, L.M., and Bergamaschi, C.T. (2021). Retroperitoneal adipose tissue denervation improves cardiometabolic and autonomic dysfunction in a high fat diet model. Life Sci. 283, 119841. https://doi.org/10.1016/j.lfs.2021.119841.

20. Li, P., Liu, B., Wu, X., Lu, Y., Qiu, M., Shen, Y., Tian, Y., Liu, C., Chen, X., Yang, C., et al. (2022). Perirenal adipose afferent nerves sustain pathological high blood pressure in rats. Nat. Commun. 13, 3130. https://doi.org/10.1038/s41467-022-30868-6.

21. Shi, Y., Li, Y., Yin, J., Hu, H., Xue, M., Li, X., Cheng, W., Wang, Y., Li, X., Wang, Y., et al. (2019). A novel sympathetic neuronal GABAergic signalling system regulates NE release to prevent ventricular arrhythmias after acute myocardial infarction. Acta Physiol. 227, e13315. https://doi.org/10.1111/apha.13315.

22. Han, S., Kobayashi, K., Joung, B., Piccirillo, G., Maruyama, M., Vinters, H.V., March, K., Lin, S.F., Shen, C., Fishbein, M.C., et al. (2012). Electroanatomic remodeling of the left stellate ganglion after myocardial infarction. J. Am. Coll. Cardiol. 59, 954–961. https://doi.org/10.1016/j.jacc.2011.11.030.

23. Zipes, D.P., and Rubart, M. (2006). Neural modulation of cardiac arrhythmias and sudden cardiac death. Heart Rhythm 3, 108–113. https://doi.org/10.1016/j.hrthm.2005.09.021.

24. Ge, Y., van Roon, L., van Gils, J.M., Geestman, T., van Munsteren, C.J., Smits, A.M.,

Goumans, M.J.T.H., DeRuiter, M.C., and Jongbloed, M.R.M. (2022). Acute myocardial infarction induces remodeling of the murine superior cervical ganglia and the carotid body. Front. Cardiovasc. Med. 9, 758265. https://doi.org/10.3389/fcvm.2022.758265.

25. Ajijola, O.A., Yagishita, D., Reddy, N.K., Yamakawa, K., Vaseghi, M., Downs, A.M., Hoover, D.B., Ardell, J.L., and Shivkumar, K. (2015). Remodeling of stellate ganglion neurons after spatially targeted myocardial infarction: Neuropeptide and morphologic changes. Heart Rhythm 12, 1027–1035. https://doi.org/10.1016/j.hrthm.2015.01.045.

26. Ibrahim, M.M. (2010). Subcutaneous and visceral adipose tissue: structural and functional differences. Obes. Rev. 11, 11–18. https://doi.org/10.1111/j.1467-789X.2009.00623.x.

27. Gan, L., Liu, D., Xie, D., Bond Lau, W., Liu, J., Christopher, T.A., Lopez, B., Liu, L., Hu, H., Yao, P., et al. (2022). Ischemic Heart-Derived Small Extracellular Vesicles Impair Adipocyte Function. Circ. Res. 130, 48–66. https://doi.org/10.1161/circresaha.121.320157.

28. Horckmans, M., Bianchini, M., Santovito, D., Megens, R.T.A., Springael, J.Y., Negri, I., Vacca, M., Di Eusanio, M., Moschetta, A., Weber, C., et al. (2018). Pericardial Adipose Tissue Regulates Granulopoiesis, Fibrosis, and Cardiac Function After Myocardial Infarction. Circulation 137, 948–960. https://doi.org/10.1161/circulationaha.117.028833.

29. Xu, J., Zhang, L., Xie, M., Li, Y., Huang, P., Saunders, T.L., Fox, D.A., Rosenquist, R., and Lin, F. (2018). Role of Complement in a Rat Model of Paclitaxel-Induced Peripheral Neuropathy. J. Immunol. 200, 4094–4101. https://doi.org/10.4049/jimmunol.1701716.

30. Jiang, G.T., Shao, L., Kong, S., Zeng, M.L., Cheng, J.J., Chen, T.X., Han, S., Yin, J., Liu, W.H., He, X.H., et al. (2021). Complement C3 Aggravates Post-epileptic Neuronal Injury Via Activation of TRPV1. Neurosci. Bull. 37, 1427–1440. https://doi.org/10.1007/s12264-021-00750-4.

31. Gibbs, J., Flores, C.M., and Hargreaves, K.M. (2004). Neuropeptide Y inhibits capsaicin-sensitive nociceptors via a Y1-receptor-mediated mechanism. Neuroscience 125, 703–709. https://doi.org/10.1016/j.neuroscience.2004.01.044.

32. Sun, L., Li, H., Tai, L.W., Gu, P., and Cheung, C.W. (2018). Adiponectin regulates thermal nociception in a mouse model of neuropathic pain. Br. J. Anaesth. 120, 1356–1367. https://doi.org/10.1016/j.bja.2018.01.016.

33. Niijima, A. (1998). Afferent signals from leptin sensors in the white adipose tissue of the epididymis, and their reflex effect in the rat. J. Auton. Nerv. Syst. 73, 19–25. https://doi.org/10.1016/s0165-1838(98)00109-x.

34. Shi, Z., Chen, W.W., Xiong, X.Q., Han, Y., Zhou, Y.B., Zhang, F., Gao, X.Y., and Zhu, G.Q. (2012). Sympathetic activation by chemical stimulation of white adipose tissues in rats. J. Appl. Physiol. 112, 1008–1014. https://doi.org/10.1152/japplphysiol.01164.2011.

35. Yu, Z., Han, J., Chen, H., Wang, Y., Zhou, L., Wang, M., Zhang, R., Jin, X., Zhang, G., Wang, C., et al. (2021). Oral Supplementation With Butyrate Improves Myocardial Ischemia/Reperfusion Injury via a Gut-Brain Neural Circuit. Front. Cardiovasc. Med. 8, 718674. https://doi.org/10.3389/fcvm.2021.718674.

36. Liu, Z., Liu, Z., Zhou, H., Zhou, Y., Xu, X., Li, Z., Guo, F., Wang, Y., Zhou, Z., Zhou, L., et al. (2023). Increased sympathetic outflow induced by emotional stress aggravates myocardial ischemia-reperfusion injury via activation of TLR7/MyD88/IRF5 signaling pathway. Inflamm. Res. 72, 901–913. https://doi.org/10.1007/s00011-023-01708-0.

37. Wang, Y., Yu, L., Meng, G., Wang, Z., Zhou, Z., Zhang, Y., Xia, H., and Jiang, H. (2018). Mast cells modulate the pathogenesis of leptin-induced left stellate ganglion activation in canines. Int. J. Cardiol. 269, 259–264. https://doi.org/10.1016/j.ijcard.2018.07.126.

38. Ajijola, O.A., Wisco, J.J., Lambert, H.W., Mahajan, A., Stark, E., Fishbein, M.C., and Shivkumar, K. (2012). Extracardiac neural remodeling in humans with cardiomyopathy. Circ. Arrhythm. Electrophysiol. 5, 1010–1116. https://doi.org/10.1161/circep.112.972836.

39. Kanazawa, H., Ieda, M., Kimura, K., Arai, T., Kawaguchi-Manabe, H., Matsuhashi, T., Endo, J., Sano, M., Kawakami, T., Kimura, T., et al. (2010). Heart failure causes cholinergic transdifferentiation of cardiac sympathetic nerves via gp130-signaling cytokines in rodents. J. Clin. Invest. 120, 408–421. https://doi.org/10.1172/jci39778.

40. Chen, D., Zhang, Y., Yidilisi, A., Xu, Y., Dong, Q., and Jiang, J. (2022). Causal Associations Between Circulating Adipokines and Cardiovascular Disease: A Mendelian Randomization Study. J. Clin. Endocrinol. Metab. 107, e2572–e2580. https://doi.org/10.1210/clinem/dgac048.

41. Wu, L.L., Zhang, Y., Li, X.Z., Du, X.L., Gao, Y., Wang, J.X., Wang, X.L., Chen, Q., Li, Y.H., Zhu, G.Q., and Tan, X. (2022). Impact of Selective Renal Afferent Denervation on Oxidative Stress and Vascular Remodeling in Spontaneously Hypertensive Rats. Antioxidants 11, 1003. https://doi.org/10.3390/antiox11051003.

42. Veiga, A.C., Milanez, M.I.O., Ferreira, G.R., Lopes, N.R., Santos, C.P., De Angelis, K., Garcia, M.L., Oyama, L.M., Gomes, G.N., Nogueira, F.N., et al. (2020). Selective afferent renal denervation mitigates renal and splanchnic sympathetic nerve overactivity and renal function in chronic kidney disease-induced hypertension. J. Hypertens. 38, 765–773. https://doi.org/10.1097/hjh.0000000000002304.

43. Lopes, N.R., Milanez, M.I.O., Martins, B.S., Veiga, A.C., Ferreira, G.R., Gomes, G.N., Girardi, A.C., Carvalho, P.M., Nogueira, F.N., Campos, R.R., et al. (2020). Afferent innervation of the ischemic kidney contributes to renal dysfunction in renovascular hypertensive rats. Pflugers Arch. 472, 325–334. https://doi.org/10.1007/s00424-019-02346-4.

STAR★METHODS

KEY RESOURCES TABLE

REAGENT or RESOURCE	SOURCE	IDENTIFIER
Antibodies		
Tyrosine hydroxylase (TH)	Servicebio	Cat#GB15182; RRID: AB_3105790
C-fos	Servicebio	Cat#GB11069; RRID: AB_3105791
TRPV1	Abcam	Cat#ab305299; RRID: AB_3105792
Choline acetyltransferase (CHAT)	Abcam	Cat#ab181023; RRID: AB_2687983
Calcitonin gene-related peptide (CGRP)	Abcam	Cat#ab283568; RRID: AB_3105794
Adiponectin (APN)	Abcam	Cat#ab181281; RRID: AB_3105795
Complement C3 (C3)	Abcam	Cat#ab200999; RRID: AB_2924273
Chemicals, Peptides, and Recombinant Proteins		
Capsaicin	MCE	Cat#HY-10448
Critical Commercial Assays		
Rat IL-6 ELISA Kit	Servicebio	Cat#GER0001
Rat TNF-alpha ELISA Kit	Servicebio	Cat#GER0004
Norepinephrine ELISA Kit	Ousaid Biotechnology Co., Ltd.	Cat# OSD-R2148
Neuropeptide Y ELISA Kit	Ousaid Biotechnology Co., Ltd.	Cat#KT30355
Deposited Data		
Transcriptomic data	This paper	SRA: PRJNA1104799
Oligonucleotides		
Calca (CGRP)	GAGGTCAACCTTGGAAAGCAGC	GGATCTCTTCTGGGCAGTGACA
APN	AGGTGTTCTTGGTCCTAAGGGTG	CCCTACGCTGAATGCTGAGTGA
C3	TCGGAACCGCTGGGAGGAG	GCACCACAGGAGGCACAGAG
NPY	ACGAATGGGGCTGTGTGGAC	CTCTGCTGGCGCGTCCTC
GAPDH	CTGGAGAAACCTGCCAAGTATG	GGTGGAAGAATGGGAGTTGCT
Software and Algorithms		
R version 4.1	N/A	https://www.r-project.org/
Prism version 9.4.1	GraphPad	https://www.graphpad.com/features
ImageJ	NIH Image	https://www.imagej.nih.gov/ij/

RESOURCE AVAILABILITY

Lead contact

Information and requests for resources and reagents should be directed to lead contact, Dr. Hong Jiang (hong-jiang@whu.edu.cn).

Materials availability

No unique materials were generated in this study.

Data and code availability

- Transcriptomic data have been deposited in the SRA and are publicly available. Accession numbers are listed in the key resources table. All data reported in this paper will be shared by lead contact upon request.
- This study did not report the original code.
- Any additional information required to reanalyze the data reported in this paper is available from the lead contact upon request.

EXPERIMENTAL MODEL AND STUDY PARTICIPANT DETAILS

Animals

Healthy male Sprague-Dawley rats (7 weeks old, weighing 250-300 g) were used in this study. All animal treatments were performed in accordance with the Guidelines for the Care and Use of Laboratory Animals (US National Institutes of Health). All experiments were approved by the Animal Welfare and Ethics Committee of Renmin Hospital of Wuhan University (No. WDRM20220901B). The animals were housed in a controlled environment with a 12-h dark/12-h light cycle, maintained at a temperature of 23°C and relative humidity of 70%. They had unrestricted access to food and water.

METHOD DETAILS

Experimental protocols

Sprague-Dawley rats were randomized into 3 groups: (1) Sham group (Sham, Sham operation with saline microinjected into the MOAT); (2) MI group (MI, MI operation with saline microinjected into the MOAT); (3) CAP group [CAP, MI operation with MOAT sensory nerve denervation (MOAT-D)]. The experimental process is illustrated in Figure 2A. The MI model was established by ligating the anterior descending coronary artery, and the CAP group immediately underwent MOAT-D. Two weeks after the model was established, echocardiography was performed to evaluate the cardiac structure and function. Electrocardiography (ECG) was performed to determine HRV to assess cardiac sympathetic activity. Blood and tissue samples were collected after the animals were euthanized for further analysis (Figure 2A). On day 28, echocardiography and ECG were performed and blood and tissue samples were collected to further evaluate the effect of CAP on ganglion remodeling (Figure 2A).

Establishment of MI model

The MI model was established using left anterior descending occlusion (LADO) surgery. All rats were anesthetized with 2% pentobarbital sodium (40 mg/kg, i.p.) and mechanically ventilated using a respirator after tracheotomy. The left third intercostal space was opened to expose the heart and the left anterior descending coronary artery was ligated using 6-0 silk sutures. The rats in the Sham group underwent left thoracotomy without LADO.

MOAT sensory nerve denervation (MOAT-D)

In the CAP group, a precise injection of high-concentration CAP was used for MOAT-D, while the Sham and MI groups received the same volume of normal saline. Following LADO surgery, an incision was made in the abdominal cavity along the linea alba to expose the greater omentum, which is situated posterior to the greater curvature of the stomach. Four distinct locations within the greater omentum adipose tissue were microinjected with CAP (33 mM, 10 μL each, Sigma Chemical Co)[41–43] or the same volume of saline. The superior mesenteric artery was traced downwards and six locations within the mesenteric adipose tissue were selected for CAP or saline microinjection. Microinjection was performed slowly, and the area was kept motionless for 5 min after the injection to prevent backflow of the agents. The abdominal cavity was closed using 4–0 silk suture.

Echocardiography

The rats were anesthetized using isoflurane (3% for induction and 2.5% for maintenance). Two-dimensional and M-mode echocardiography was performed using a High-Resolution Imaging System (GE Vivid E95, USA) equipped with a 12-MHz probe (12S) to assess cardiac function. The left ventricular EF, FS, and LVID, including LVIDs and LVIDd, were measured and calculated by the same operator.

Measurement of the HRV

Body surface ECG was recorded under anesthesia (2.5% pentobarbital sodium, i.p.) and used for HRV assessment. The frequency domain parameters, comprising LF (0.20-0.75 Hz), HF (0.75-2.5 Hz), and the LF/HF ratio was analyzed by LabChart software (version8.0, AD Instruments).

Histological assessment

At the end of the experiment, the heart, brain, and SCG were promptly collected from each rat, fixed in 4% formalin and embedded in paraffin. Paraffin blocks were cut into 5-μm sections for further analysis. To determine cardiac remodeling, heart tissue sections were stained with Masson's trichrome (Masson dyeing liquor from Servicebio). TUNEL staining (TUNEL Detection Kit from Servicebio) was used to assess cardiomyocyte apoptosis after MI. Immunofluorescence labeling for TH (Servicebio) and c-fos (Servicebio) was used to assess neural activation in the SCG and PVN. The nuclei were stained with 4′,6-diamidino-2-phenylindole (DAPI). The expression levels of TRPV1 (Abcam, UK) in the DRG were detected by immunohistochemistry. Additionally, immunohistochemical labeling of ChAT (Servicebio) and TH was performed in the SCG to assess remodeling. All analyses were performed quantitatively using NIH ImageJ software.

qRT-PCR analysis

Samples from MOAT were homogenized, and total RNA was extracted using TRIzol Reagent (Invitrogen, USA). The RNA concentration was evaluated using a NanoDrop 2000 spectrophotometer. RNA was reverse-transcribed using the RevertAid First Strand cDNA Synthesis Kit (Thermo, MA, USA). qRT-PCR analysis was performed using the FastStart Universal SYBR Green Master Mix (Servicebio, China) to evaluate the expression of relevant genes. GAPDH was used for normalization. The gene expression levels were determined using the 2-ΔΔCT method. The mRNA expression levels of CGRP, APN, C3, and NPY were detected. Primer sequences are listed in the key resources table.

RNA sequencing (RNA-Seq)

For RNA sequencing (RNA-Seq) studies, MOAT samples from the Sham and MI groups were rapidly excised and immediately frozen in liquid nitrogen for further analysis. The BGSEQ-500 (BGI-Shenzhen, China) platform was used for gene sequencing to obtain raw reads. The clean reads were mapped to the rat genome (*Rattus_norvegicus*, UCSC, rn6) using HISAT2 (Hierarchical Indexing for Spliced Alignment of Transcripts), and Bowtie2 (version 2.2.5) was used to align the clean reads for the reference coding gene set. The expression was calculated as fragments per kilobase million (FPKM). The DESeq algorithm was then used to identify differential gene expression between groups. R software was used to analyze the gene expression heatmap, KEGG pathway and enrichment, and GO term enrichment. GSEA was performed using GSEA official software package. The P-value was adjusted using the false discovery rate (FDR), and the adjusted P-value was designated as the Q-value. The significance level was set at a Q-value of ≤ 0.05.

ELISA

Blood samples were obtained by collecting 5 mL of peripheral venous blood and centrifugation at 3,000 rpm for 15 min (4°C). Serum was collected and stored at –80°C for further analysis. The concentrations of IL-6, TNF-α, NE, and NPY were determined using ELISA kits (GER0001, GER0004, Servicebio, China; OSD-R2148, OSD-KT30355 Ousaid, China) according to the manufacturer's instructions.

Western blotting

Western blot analysis was used to assess CGRP expression in the DRG and APN expression in the MOAT. The tissues were rapidly removed, frozen in liquid nitrogen, and stored at –80°C for further analysis. After tissue homogenization in buffer on ice, supernatants were collected as the total lysate. Equal amounts of homogenized proteins were separated using 10% SDS-PAGE, transferred onto polyvinylidene fluoride membranes (PVDF, Millipore, USA), and blocked with 5% skim milk at room temperature for 1 h. The membranes were then incubated overnight with primary antibodies at 4°C. The primary antibodies used were anti-CGRP (Abcam, UK), anti-APN (Abcam, UK), anti-C3 (Abcam, UK), and GAPDH (Abcam, UK). After washing, the membranes were incubated with the secondary antibody at room temperature for 1 h. The secondary antibody was horseradish peroxidase (HRP)-conjugated goat anti-rabbit (1:3,000, Elabscience, China). Band intensities were analyzed using the Odyssey Imaging System (LICOR Biosciences, USA). The expression levels of the target proteins were normalized to those of GAPDH.

QUANTIFICATION AND STATISTICAL ANALYSIS

Statistical analysis

Data are presented as mean $\pm$ standard error of the mean (SEMs). Statistical differences were assessed using one-way analysis of variance (ANOVA), followed by Tukey's multiple comparison post-hoc test. All statistical analyses were performed using GraphPad Prism 9 software. P-values < 0.05 were considered statistically significant.